7

Determination of Thermodynamic and Transport Properties of Non-Stoichiometric Oxides

Mauvy Fabrice[1] and Fouletier Jacques[2]
[1]*ICMC Bordeaux, CNRS, Université de Bordeaux, UPR 9048, 33608 Pessac, Cedex,*
[2]*LEPMI, UMR 5279, CNRS, Grenoble INP, Université de Savoie, Université Joseph Fourier, BP75. 38402 Saint Martin d'Hères, France*

1. Introduction

The purpose of this chapter is to describe methods for determining the oxygen stoichiometry (bulk and surface oxygen activities) and transport properties in non-stoichiometric oxides using solid electrolyte cells. These oxides are generally referred to as "*mixed ionic-electronic conductors*" (*MIEC*). It is customary to consider that in a MIEC, the ionic or electronic transport number is higher than 0.01 and that the total electrical conductivity is sufficiently high, i.e., higher than 10^{-5} S.cm^{-1}. Emphasis will be given on sources of error. Devices for overcoming these sources of error will be described. As the aim of this chapter is limited and cannot be an exhaustive review, the readers are referred to excellent general handbooks dealing with solid state electrochemistry, with chapters devoted to electrochemistry of non-stoichiometric oxides [Gellings & Bouwmeester, 1997; Kharton, 2011; Rickert, 1982; Sorensen, 1981] or review papers [Heyne, 1982; Weppner & Huggins, 1978].

2. Control and measurement of oxygen activity

Precise control and monitoring of the oxygen pressure in the experimental chamber is required for the determination of thermodynamic and transport properties in MIECs. Electrochemical devices have been developed since more than thirty years, allowing the control of the oxygen pressure in the 1 - 10^{-27} bar range in various gas mixtures or under partial vacuum. Solid electrolyte microprobes have also been proposed for the local determination of the oxygen activity on the surface of a non-stoichiometric oxide.

2.1 Measurement of oxygen pressure in a gas phase and under partial vacuum

The conventional oxygen sensor, shown Figure 1 a, is based on a closed yttria-stabilized zirconia tube [Kleitz et al., 1992]. The electrodes are made of platinum paste. The outer electrode, in contact with air, forms the reference electrode. The cell *emf* obeys the Nernst law:

$$E_{th} = \frac{RT}{4F} \ln \frac{P_{O_2}}{P_{(O_2)_{air}}} = \frac{RT}{4F} \ln \frac{P_{O_2}}{0.2} \quad (1)$$

A miniaturized sensor (Figure 1 b) with enclosed metal-metal oxide reference system (Pd-PdO, Co-CoO) has been developed and commercialized[1] [Fouletier & Vitter, 1980]. The main advantage of this device concerns the possibility of in situ measurements without circulation of the analyzed gas.

It has been shown that under partial vacuum or for high temperature operation, the sensor could become inaccurate due to the disturbing effect of the oxygen semipermeability flux through the zirconia tube, reaching the measuring electrode. To overcome the problem, it has been proposed to use the "zirconia point electrode" shown in Figure 1 c. The platinum measuring electrode is replaced by a conical piece of zirconia (see also Figure 4 a) pressed in contact with the inner surface of the zirconia tube, which is not platinized. The actual measuring electrode is a platinum coating deposited on the top of the zirconia probe. In this design, due to the shape of the probe, the oxygen semipermeability flux does not reach the measuring electrode since the current follows the path of lowest resistance. Consequently, the measuring electrode remains in equilibrium with the gas phase. As developed in Section 2.2.1, this zirconia point electrode can be used for the measurement of oxygen activity on the surface of a non-stoichiometric oxide.

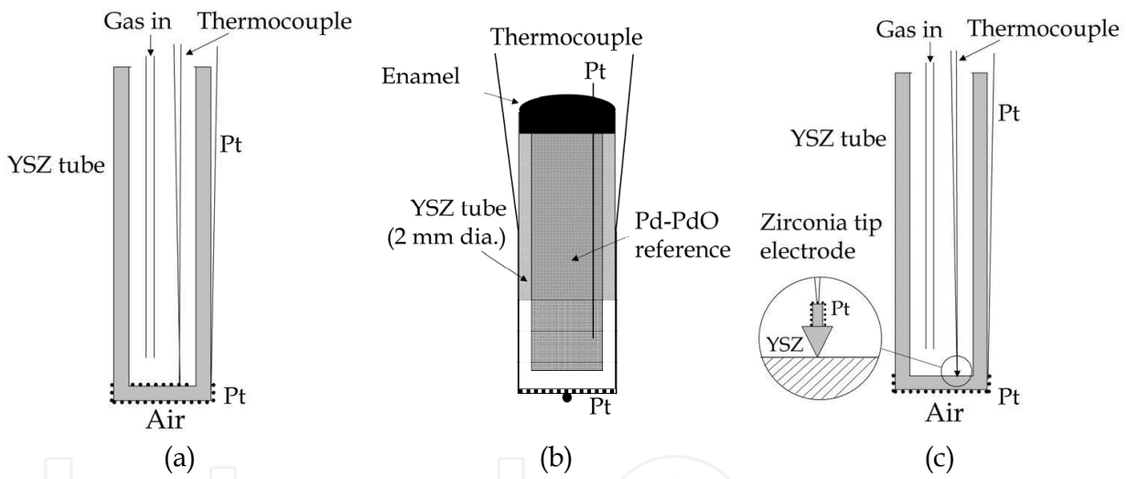

Fig. 1. Schematic drawing of oxygen sensors: (a) conventional type (air reference electrode), (b) minisensor with Pd-PdO reference system, (c) sensor with zirconia tip measuring electrode, [Fouletier, 1982/83].

2.1.1 Pump-sensor device

This device is widely used for the control and monitoring of oxygen content in gas mixtures flowing in the experimental chamber. The gas circuit is schematized in Figure 2 a. When nominally pure gases (Ar, N_2, He, etc.) are used, according to the Faraday law, the oxygen mole fraction X in the flowing gas obeys the following equation:

$$X = X° + 0.209\ I/D \tag{2}$$

[1] SETNAG, Marseille

where X° is the oxygen mole fraction in the gas supplied to the pump, D is the gas flow rate in $L.h^{-1}$ NTP and I is the current intensity in A. As shown in Figure 2 b, the theoretical equation (2) is verified in the 10^{-7} – 1 mole fraction range: the oxygen mole fraction is determined by the oxygen sensor (using Nernst equation (1)) for various current intensities I passing through the pump [Fouletier et al., 1975].

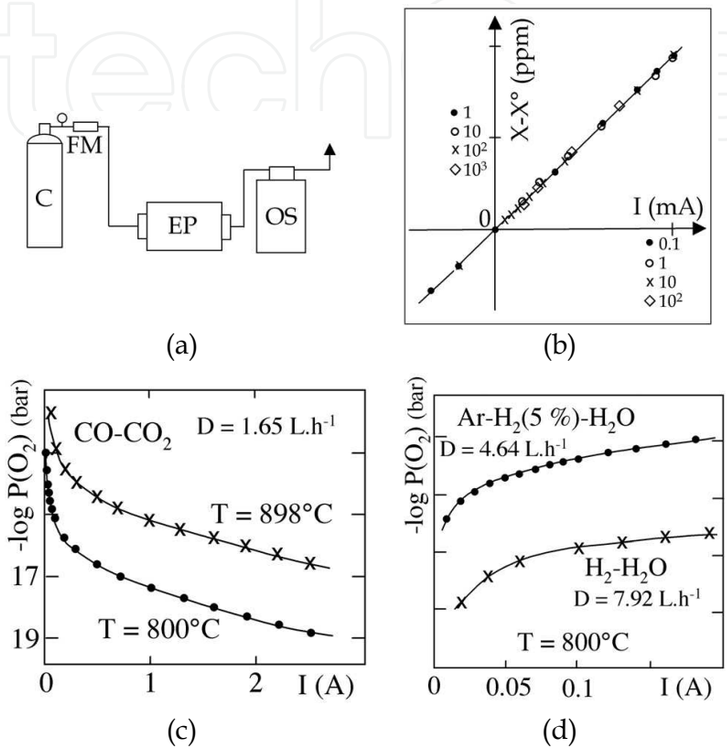

Fig. 2. (a): Gas circuit, C: gas container, FM: flowmeter, EP: electrochemical pump, OS: oxygen sensor; (b): Faraday's law test (T_{sensor} = 900°C, X° = $9.1x10^{-7}$, D = 11.1 $L.h^{-1}$, experimental slope: $1.96x10^{-2}$ A^{-1}, theoretical slope: $1.88x10^{-2}$ A^{-1}); (c): Reduction of flowing carbon dioxide for two temperatures of the sensor, (d): Oxidation of Ar – H_2 (5 %) mixture and pure hydrogen. The full lines are the theoretical curves, according to equations (3) and (4) [Caneiro et al., 1981; Fouletier et al., 1984].

The same device can be used for monitoring the composition of CO_2-CO and Ar-H_2O-H_2 mixtures. In that case, pure (H_2, CO_2) or premixed gases, such as Ar – 5 % H_2 are used. According to the Faraday's law, the equilibrium oxygen pressure vs. the current intensity passing through the pump obeys the following equations:

$CO\text{-}CO_2$ mixture

$$P_{O_2} = \left(2.392\frac{D}{I} - 1\right)^2 \exp\left(21.05 - \frac{68150}{T}\right) \text{(in bar)} \quad (3)$$

Ar-H_2-H_2O mixture

$$P_{O_2} = \left(2.392q\frac{D}{I} - 1\right)^{-2} \exp\left(13.278 - \frac{59571}{T}\right) (\text{in bar}) \quad (4)$$

where q is the hydrogen mole fraction in the feed gas, and T is the absolute temperature in the experimental chamber.

The association of an electrochemical oxygen pump and an oxygen sensor allows the monitoring of oxygen partial pressure in a flowing gas in the range 1 bar – 10^{-27} bar with an accuracy of 2 %.

2.1.2 Oxygen pressure domains of ideal response

It should be pointed out that the accuracy of the equilibrium oxygen pressure control depends on the *buffer capacity* δ of the gas. The buffer capacity can be defined as the number of moles of oxygen required for changing the chemical potential of 1 kJ/mole of gas. The variation of δ with oxygen pressure, at various temperatures, for Ar-O_2 and CO_2/CO mixtures is given in Fig. 3. It has been shown previously that the buffer capacity of the gas has to be higher than 10^{-6} mole, at 800°C. Consequently, at this temperature, the pressure domains in which the oxygen pressure is accurately controlled are: 1 - 10^{-6} bar in Ar-O_2 mixtures and 10^{-10} - 10^{-27} bar in CO-CO_2 mixtures. Obviously, these pressure domains depend on temperature. The same type of curve is obtained with H_2/H_2O mixtures.

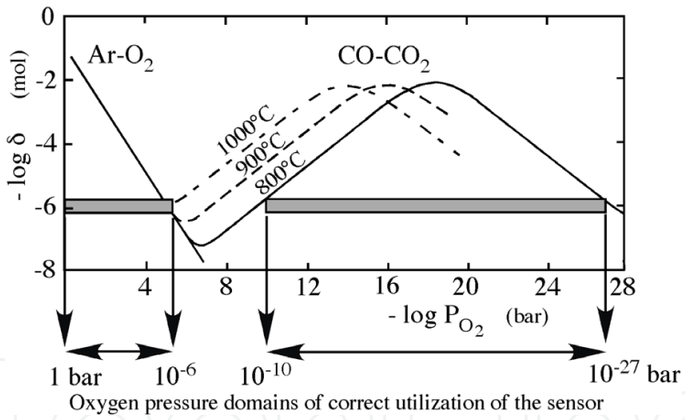

Fig. 3. Variation of the buffer capacity of inert gas-O_2 and CO-CO_2 mixtures, with indication of the oxygen pressure domains of correct utilization of the oxygen sensor at 800°C [Fouletier, 1982/83].

2.2 Control and measurement on an oxide surface

Basically, the oxide ion activity in a MIEC can be determined using the electrochemical cell:

Pt - Reference system / oxide electrolyte / MIEC - Pt. The measurement of the emf of the electrochemical chain allows the determination of the oxygen activity in the MIEC. The following sections are devoted to the description of devices allowing the determination of the oxide activity on the surface of a MIEC, and of the deviation from equilibrium of the oxide surface.

2.2.1 Metallic and solid electrolyte probes

It has been shown that in case of oxygen transfer through the studied sample, the activity of oxygen $a^*_{O_2}$ on the surface of the pellet can be noticeably different from that in the bulk. The oxygen activity $a^*_{O_2}$ can by defined as an equivalent oxygen pressure $P^*_{O_2}$. This surface activity can be measured using a ceramic point electrode (either a zirconia- or a ceria-based microprobe, Figure 4 a), as depicted in Section 2.1. The schematic drawing of the cell is given, Figure 4 b. The oxygen activity on surface of the sample (MO) results from the balance of the oxygen adsorption and desorption fluxes and the oxygen flux through the sample. Consequently, the oxygen activity on the surface of the sample can be very different from the oxygen partial pressure in the gas ($a^*_{O_2} = P^*_{O_2} \neq P_{O_2}$) and it can be written:

$$\frac{1}{2}O_{2(surface)} + 2e^-_{MO} = O^{2-}_{MO} \text{ leading to : } \frac{1}{2}\mu^*_{O_2} + 2\mu^{MO}_e = \mu^{MO}_{O^{2-}} \quad (5)$$

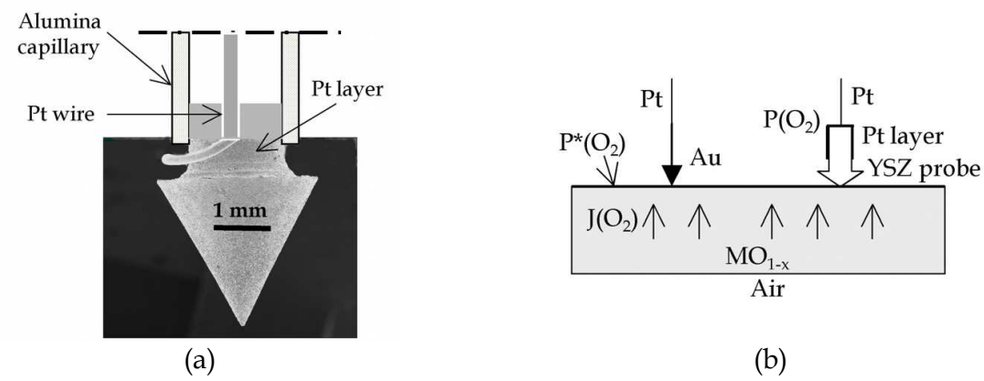

(a) (b)

Fig. 4. (a): Ceramic point electrode; (b): Schematic drawing of the cell allowing the measurement of the oxygen activity on the surface of a MIEC.

The potential change in the electrochemical chain can be summarized as ($E = \phi^{Pt\text{-}I} - \phi^{Pt\text{-}II}$):

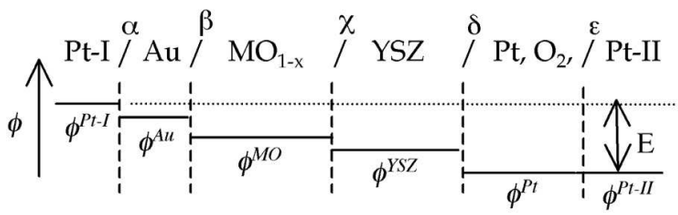

Fig. 5. Qualitative variation of the potential within the chain.

Gold is used as metallic point electrode due to its poor catalytic activity for oxygen electrode reaction; consequently, gold can be considered as an electronic probe on the MIEC and: $\tilde{\mu}^{Au}_e = \tilde{\mu}^{MO}_e$. It is also assumed that there is no oxygen flux at the interface between the ceramic point electrode and the pellet ($\tilde{\mu}^{MO}_{O^{2-}} = \tilde{\mu}^{YSZ}_{O^{2-}}$). The MIEC surface is considered as an equipotential. The emf E of the chain can be easily obtained from the following assumptions:

- Electronic equilibrium at interfaces α and β: $\tilde{\mu}^{Pt-I}_e = \tilde{\mu}^{Au}_e = \tilde{\mu}^{MO}_e$

- Ionic equilibrium at the interface χ: $\tilde{\mu}_{O^{2-}}^{MO} = \tilde{\mu}_{O^{2-}}^{YSZ}$
- Electrochemical equilibrium at the interface δ:

$$\frac{1}{2}O_{2(gas)} + 2e_{Pt}^{-} = O_{YSZ}^{2-} \quad \text{leading to}: \frac{1}{2}\mu_{O_2} + 2\tilde{\mu}_e^{Pt} = \tilde{\mu}_{O^{2-}}^{YSZ}.$$

- Electronic equilibrium at the interface ε: $\tilde{\mu}_e^{Pt-II} = \tilde{\mu}_e^{Pt}$

Considering that $\mu_{O_2} = RT \ln P_{O_2}$ and $\mu_{O_2}^{*} = RT \ln P_{O_2}^{*}$ we obtain easily the emf E of the chain:

$$E = \phi^{Pt-I} - \phi^{Pt-I1} = \frac{RT}{4F} \ln \left[\frac{P_{O_2}^{*}}{P_{O_2}} \right] \tag{6}$$

Obviously, if the surface of the sample is in equilibrium with the gas phase, the emf is nil. Provided the oxygen pressure in the gas phase near the surface is known (as an example using a microsensor described in Section 2.1), the oxygen activity on the surface can be determined (see Section 4.1). Similar designs using calcia-stabilized zirconia cells have been tested for continuous monitoring of oxygen activity on the surface of growing scale during high temperature oxidation of metals [Akida et al., 2008].

2.2.2 Oxygen minisensor

Mini-probes (Figure 6) have been developed for the determination of thermodynamic properties of MIEC as a function of composition. Zirconia- or thoria-based tubes, a few mm in diameter, have been used. A metal-metal oxide system serves as a reference. Such cells have been used for the measurement of oxygen potential in urania-based solid solutions or for continuous control of oxygen redistribution in UO_{2+x} under a thermal gradient [Ducroux et al., 1980; Une & Oguma, 1982].

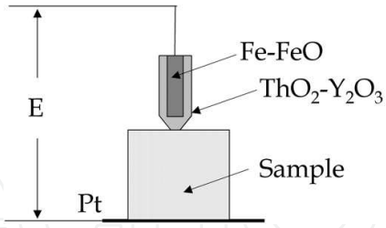

Fig. 6. Solid electrolyte mini-probe.

3. Determination of nonstoichiometry in oxides

Various methods based on the measurement of different physico-chemical characteristics have been developed. Most of the methods measure changes of the non-stoichiometry ratio x; however, with the help of a defect model, the absolute value of x can often be obtained [Riess & Tannhauser, 1982]. Thermogravimetry under controlled oxygen pressure is the most widely used method [Caneiro et al., 1982, 2011; Kharton et al.]. Other methods are based on the coulometric titrations. The oxygen activity in MIECs can also be determined using potentiometric cells involving a solid electrolyte. In the following sections, only the techniques involving solid electrolytes designs will be described.

3.1 Thermogravimetric investigation under controlled oxygen partial pressure

Thermal stability and oxygen content versus temperature and oxygen partial pressure are very important parameters in the case of non-stoichiometric compounds. Oxygen non-stoichiometry (δ) is generally measured using electronic microbalances under controlled atmospheres [Kharton et al., 2008; Tsipis et al., 2008]. About 1 g of powder sample is placed in a silica basket suspended by platinum wires from the beam of the microbalance. The oxygen partial pressure is controlled by the introduction of gas mixtures (Ar-O_2, Ar-H_2, dry or wet) into the sample chamber [Nakamura et al., 2009a], [Kiselev et al., 2011; Nakamura et al., 2009b]. First of all, the equilibrium between the sample and the surrounding gas phase is checked by controlling that both the weight of the sample and the oxygen partial pressure (recorded by a zirconia sensor introduced into the sample chamber) reached constant value. Figure 7a shows a typical weight change curve of $Nd_{2-x}NiO_{4+\delta}$ in Ar-H_2 mixed atmosphere to determine the starting oxygen content of the sample [Zhao et al., 2008].

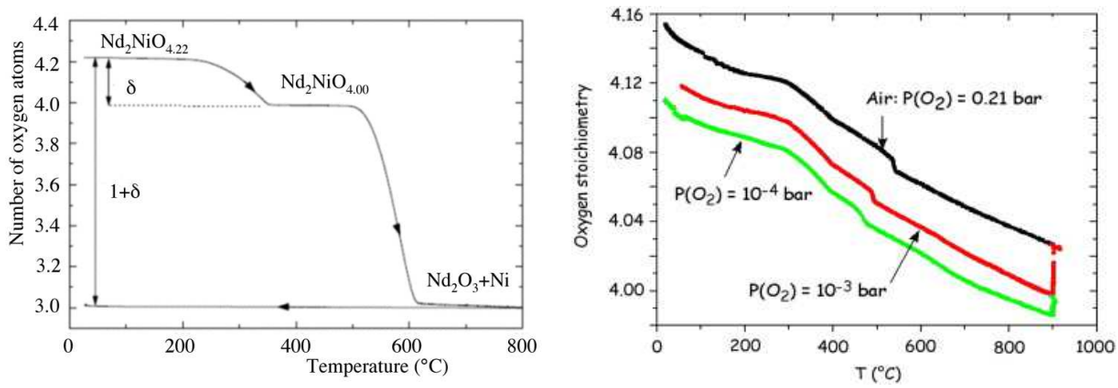

(a) (b)

Fig. 7. Thermogravimetric analysis (TGA) (a) weight loss measurements during reduction of $Nd_2NiO_{4.22}$ in H_2 (5%) / Ar atmosphere ; (b) oxygen stoichiometry versus temperature of $Nd_{1.95}NiO_{4+\delta}$, under three oxygen pressures.

The change in oxygen content is determined from variation of the weight of the sample Δw_S according to the following relation:

$$\Delta\delta = (M_S/M_O).(\Delta w_S/w_S) \quad (7)$$

where $\Delta\delta$, M_S, M_O, w_S are the variation of oxygen nonstoichiometry, the molar formula weight of the sample and oxygen atom and the weight of the specimen, respectively. The experimental error due to the buoyancy is negligibly small compared to the weight variation of the sample due to release or incorporation of oxygen.

In the case of figure 7a, two weight changes are observed. The first one occurring at 350°C corresponds to the loss of interstitial oxygen and the reduction of Ni^{3+} to Ni^{2+}. The second weight loss is assigned to the total reduction of $Nd_2NiO_{4+\delta}$ to Nd_2O_3 and Ni metal. The absolute value of the oxygen content is determined from the weight change of the sample during the decomposition in H_2 atmosphere. The decomposition reaction can be expressed by:

$$Nd_{2-x}NiO_{4+\delta} \rightarrow (2-x)/2\ Nd_2O_3 + Ni + (2+2\delta+3x)/2\ O \quad (8)$$

From the weight change, the δ value is deduced and the Ni^{3+} concentration can be estimated. This mixed valency parameter can be linked to the electronic conductivity of the compound.

The change of molar Gibbs energy ΔG° for reaction (8) represents the partial molar Gibbs energy of oxygen atoms per 1 mol and can be expressed as follows [Caneiro et al., 2011; Patrakeev et al 1995]:

$$\Delta G° = -0.5\ RT\ Ln\ PO_2 \quad (9)$$

where R, T and PO_2 are the gas constant, the temperature and the oxygen partial pressure, respectively. Taking into account the Gibbs-Helmholtz equation, and equation (9), the changes of standard partial molar enthalpy ΔH° and entropy ΔS° of oxygen release process per 1 mol of oxygen atoms can be deduced from equations (10) and (11) respectively:

$$\Delta H° = -\frac{R}{2}\left[\frac{\partial \ln P_{O_2}}{\partial(1/T)}\right]_\delta \quad (10)$$

$$\Delta S° = \frac{R}{2}\left[\frac{\partial(T.\ln P_{O_2})}{\partial T}\right]_\delta \quad (11)$$

In order to determine the standard thermodynamic quantities, experimental dependences of the non-stoichiometry (δ) versus temperature and oxygen partial pressure are determined (see Fig. 7b) [Mauvy et al., 2009]. If the plots into the coordinates R/2 Ln PO_2 vs. $(1/T)_\delta$ and RT/2 Ln PO_2 vs. $(T)_\delta$ give linear relationship within the values of δ studied, it allows to access to standard partial molar enthalpy ΔH° and entropy ΔS° (Fig. 8a). This linear behaviour indicates that the values of standard thermodynamic quantities are essentially independent of the temperature in the working temperature range. These values can be estimated from linear regression coefficients at given oxygen content. Figure 8b shows the calculated values of the standard enthalpy ΔH° for oxygen release process for $Nd_{1.95}NiO_{4+\delta}$ compound.

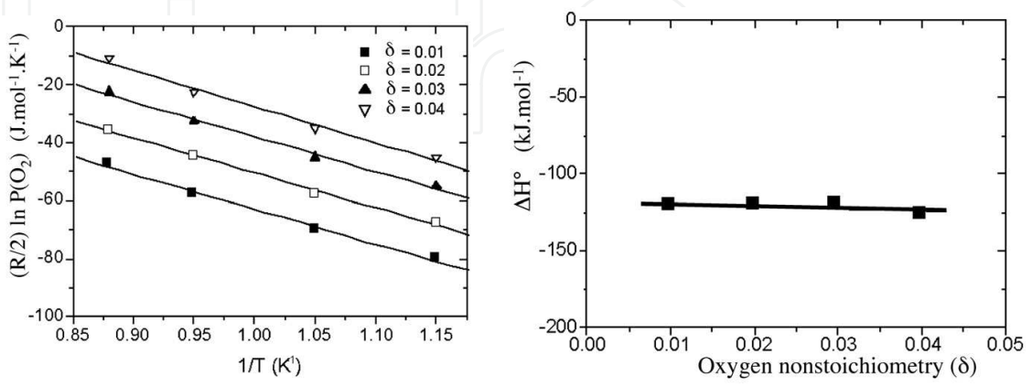

(a) (b)

Fig. 8. (a) R/2 Ln PO_2 vs. $(1/T)_\delta$ plots of $Nd_{1.95}NiO_{4+\delta}$; (b) partial molar enthalpy of $Nd_{1.95}NiO_{4+\delta}$.

It can be noticed that a linear behaviour of both thermodynamic parameters ΔH° and ΔS° versus δ, can be related to a random distribution of non-interacting point defects as components of ideal solution. Generally, when the nonstoichiometry increases, noticeable deviation from linearity can be observed. In the case of $Nd_{1.95}NiO_{4+\delta}$ oxide, ideal-solution-like state means that the interaction among defect species is nearly constant regardless of the defect concentration.

3.2 Pump-sensor device

The pump-sensor device described in section 2.1.1 can be used for the determination of the stoichiometry ratio in oxides using the device shown Fig. 9 a [Meas et al., 1978].

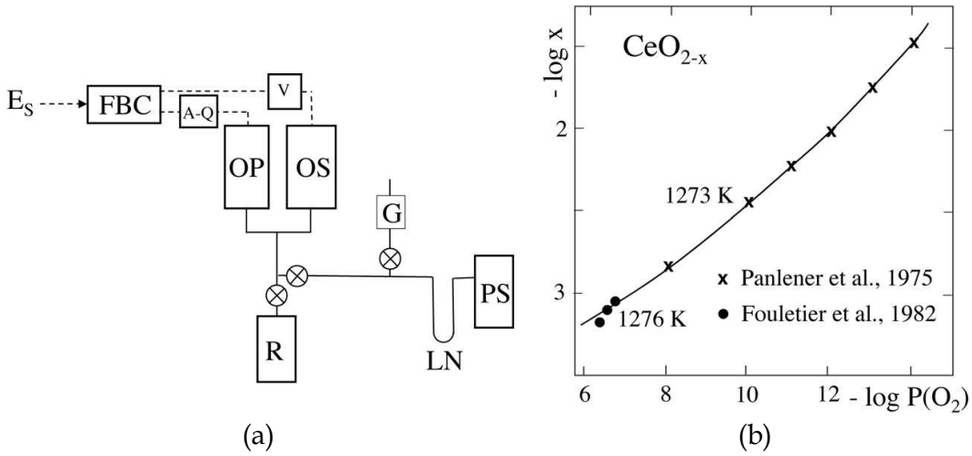

Fig. 9. (a): Experimental device for the study of gas-solid reaction under constant oxygen pressure using a pump-sensor device, G: vacuum gauge, LN: liquid nitrogen trap; (b): Variation of the stoichiometry ratio of CeO_{2-x} at 1273 K.

The experimental reactor R is connected to an oxygen sensor OS (using a zirconia probe as measuring electrode), an oxygen pump OP and a mechanical pumping system PS. A feed-back controller FBC compares the sensor emf E given by the sensor to a set value E_S and adjust the oxygen pressure in the experimental vessel by passing an appropriate current through the electrochemical pump. As a preliminary treatment, the system was initially outgassed under a pressure lower than 10^{-8} bar and then equilibrated with a well-controlled low oxygen pressure, typically 10^{-7} bar. Starting from this equilibrium state, a typical experiment is simply performed by changing the set voltage E_S and recording the resulting pumping current passing through the oxygen pump and its integral which is proportional to the oxygen amount exchanged between the solid and the gas. Following an identical procedure, measurements were first carried out without sample in the reaction vessel. The quantities of oxygen involved in the gas-solid equilibrium are calculated by difference. This device has been used for oxygen adsorption studies on zeolite or on stabilized zirconia [Meas et al. 1978]. As an example, in figure 9 b, is plotted the variation of the stoichiometry ratio of CeO_{2-x} as a function of oxygen partial pressure, at 1273 K [Fouletier et al., 1982].

3.3 Coulometric titration

The coulometric titration method can be defined as charge controlled mass transfer of mobile component between electrodes of electrochemical cell. This method is a very sensitive control of the composition of the nonstoichiometric phase, combined with emf measurements that yield very accurate thermodynamic information [Tretyakov et al., 1997].

As reported in Fig. 10, an yttria stabilized zirconia tube is used as electrolyte for a galvanic cell [Mizusaki et al., 1991; Nakamura et al., 2009a]. Platinum paste is painted on the outside of the tube to stick the Pt mesh whereas Pt mesh is attached to the sample powder as the inside electrode.

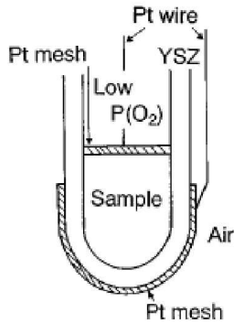

Fig. 10. Schematic diagram of the coulometric titration cell.

After evacuation and fulfilment with Ar gas procedures, the amount of oxygen, which is extracted or incorporated to the sample, is controlled by the electric charge passed through the cell. After specified amount of electric charge is applied, the electromotive force is measured to determine the equilibrium oxygen partial pressure in the tube. By considering that the amount of oxygen inside the tube is negligibly small, the oxygen amount, which migrated between the sample oxide and the gas phase, is small enough to be neglected. Then, $\Delta\delta$ can be calculated according to the relation:

$$\Delta\delta = (I.t) / (2.F.M_S) \quad (12)$$

where I , t, F and M_S are the current, the time, the Faraday constant and the molar weight of the sample, respectively.

Typical examples of coulometric titration curves are reported in Fig. 11 for $La_2NiO_{4+\delta}$ compound at different temperatures [Nakamura et al, 2009b].

It can be noticed that data points near the plateau of δ versus log PO_2 region contain larger uncertainty than other data points because equilibrium potential varies easily by the small variation of oxygen content near the plateau region. According to Wagner theory, the slope of the δ versus log PO_2 curve for nonstoichiometric compounds shows minimum value at the stoichiometric composition [Wagner, 1971].

Investigations with oxygen concentration cells revealed that the major problem is a non-electrochemical transport of oxygen through oxide ion electrolytes. Such leakage introduces uncontrolled and excessive changes in the oxide composition and appears to be the principal cause of instability.

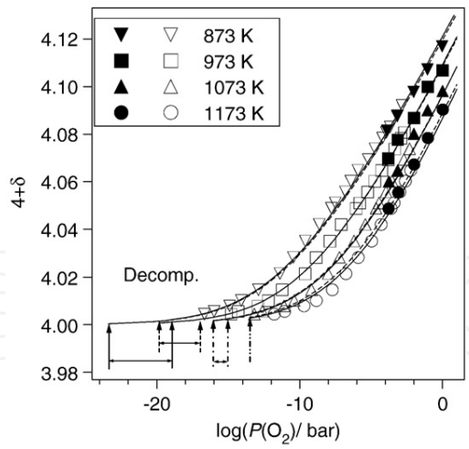

Fig. 11. Oxygen nonstoichiometry of $La_2NiO_{4+\delta}$. Open symbols and closed symbols are measured by coulometric titration and TG analysis respectively [Nakamura et al., 2009b].

3.4 Gas release method

The stoichiometry ratio in a non-stoichiometric oxide can be monitored by passing a current through it [Fouletier & Kleitz, 1978; Fouletier et al, 1982]. The experimental set-up is schematized, Fig. 12a. It consists of an inert gas cylinder, an oxygen pump, the experimental vessel and an oxygen sensor. The sample is a cylindrical pellet with platinum electrodes deposited on its bases. The sample is electrochemically reduced by passing a direct current. The amount of oxygen extracted from the sample, and the corresponding variation of the stoichiometry ratio, is determined by integration of the oxygen content deduced from the downstream oxygen sensor emf (Fig. 12b) [Levy et al., 1988].

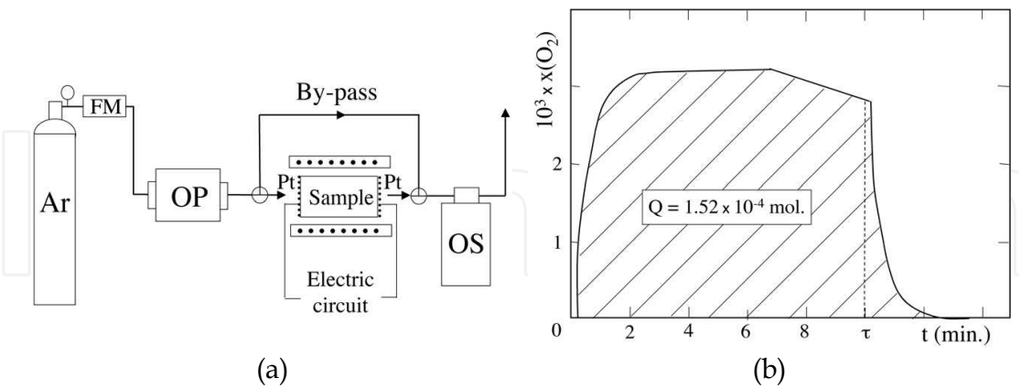

(a) (b)

Fig. 12. (a): Experimental set-up for the monitoring of the stoichiometry ratio in a MIEC, FM: flowmeter, OP: oxygen pump, OS: oxygen sensor; (b): Variation of the oxygen mole fraction $x(O_2)$ in the flowing gas during reduction process (ZrO_2 - 12 m/o Y_2O_3, T = 1015 K, $I_{reduction}$ = 0.01 A, gas flow rate : 1.8×10^{-3} mol.s^{-1}).

As an example, for the oxide $Zr_{1-y}Y_{2y}O_{2+y-x}$, (y is the dopant concentration), the stoichiometry ratio x is calculated from the equation:

$$x = 0.4\frac{M_S D}{m(1+y)V_m}\int_0^t\left(\exp\left[\frac{4FE(t)}{RT}\right]-\exp\left[\frac{4FE(0)}{RT}\right]\right)dt \quad (13)$$

where E(t) represents the emf of the oxygen sensor during the reduction process, E(0) is the sensor emf before electrochemical reduction, D the gas flow rate, V_m the volume of a mole of gas, M_S the sample molecular weight, and m the sample weight.

3.5 EMF method

According to the pioneering works of Kiukkola & Wagner [Kiukkola & Wagner, 1957], the electrochemical chain is the following: Pt - Reference system / oxide electrolyte / MIEC – Pt. As described in Section 2.2.1, the emf of the cell allows the measurement of the oxygen activity in the MIEC, provided that there is no mass transfer through the oxide surface. The reference system is either a gas (pure oxygen, air) or a metal-metal oxide mixture (Fe-FeO, Cu-Cu_2O, Pd-PdO, etc.). Examples of measurements on non-stoichiometric oxides are numerous [Mari et al., 1977; Nakamura & Fujino, 1987; Otobe et al., 2009; Porat & Riess, 1994].

The two main problems concern the reactivity between the MIEC and the solid electrolyte and the appearance of electronic conductivity in the solid electrolyte inducing polarization phenomena. The appropriate choice of the solid electrolyte can noticeably reduce the chemical reactivity: as an example, ceria-based electrolyte or apatite is less reactive than stabilized zirconia [Mauvy et al., 2009]. Double-electrolyte cells have been proposed to extend the oxygen activity range of thermodynamic cell measurements compared to the range of a single-electrolyte cell arrangement [Shores & Rapp, 1971; Tretyakov & Muan, 1969].

We will focus on the use of cone-shaped MIEC. The experimental set-up is schematized, Figure 13a, and a photograph of a nickelate point electrode is shown, Figure 13b. Air is used as a reference electrode, and the cone-shaped MIEC is gently pressed in contact with the

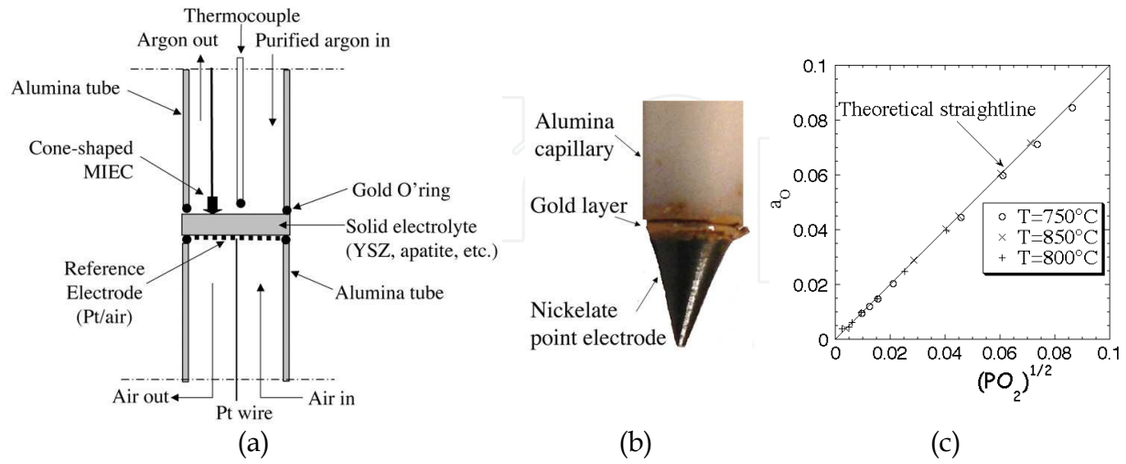

(a) (b) (c)

Fig. 13. (a): Experimental set-up for emf measurement; (b): Photograph of a nickelate point electrode ($Ni_{1.95}NiO_{4+\delta}$); (c): Variation of the oxygen activity coefficient in the nickelate as a function of temperature for various oxygen activity values in the gas phase [Mauvy et al., 2009].

solid electrolyte (zirconia-based pellet, apatite, etc.). If available, a solid electrolyte closed-end tube can be used. The main advantages concern the possibility of simultaneous measurements with various MIEC materials, the ease to handle, the reactivity between the MIEC and the solid electrolyte is minimized, a reduced response time to reach thermodynamic equilibrium.

As an example, in Figure 13c is plotted the variation of the oxygen activity (a_O) in the nickelate phase $Ni_{1.95}NiO_{4+\delta}$ as a function of the activity of oxygen in the gas ($P_{O_2}^{1/2}$). The equilibrium between the nickelate and the gas phase is observed in the whole investigated temperature range.

4. Transport properties investigations in MIEC oxides

Because of the charge equilibrium within the oxide, the electronic partial conductivity (electrons or holes) σ_{el} and the ionic partial conductivity σ_i are linked to the oxygen non-stoichiometry and, consequently, are two key parameters characterizing a MIEC. The methods developed for deconvoluting the ionic and electronic contributions to the total conductivity of a MIEC allow either the measurement of the partial conductivities, the diffusion coefficient of mobile defects or the transport numbers, either t_{el} or t_{ion}. Only the methods involving a solid electrolyte cell are briefly described. Reviews papers can be referred [Heyne, 1982; Rickert, 1982; Riess, 1997; Weppner & Huggins, 1978].

4.1 Oxygen permeation

Assuming that there is no oxygen gradient in the gas phase, the overall oxygen permeation rate through a non-stoichiometric oxide may be schematically decomposed into three elementary steps: ionic defect bulk diffusion (step 1), surface exchange between oxygen and oxygen vacancies (step 2 (high pressure side, $P_{O_2}^{rich}$) and step 3 (low pressure side, $P_{O_2}^{lean}$)). As previously proposed [Bouwmeester et al., 1992] the membrane may be divided into three zones, as schematically shown in Fig. 14a. $P_{O_2}^{rich}$ and $P_{O_2}^{lean}$ are the oxygen pressure in the gas phase, $P_{O_2}^{*rich}$ and $P_{O_2}^{*lean}$ are the actual corresponding oxygen activities on both surfaces of the membrane.

The experimental cell for oxygen permeation measurements, including metallic and ceramic point electrodes is shown Figure 14 b.

The chemically driven oxygen flux through a mixed-conducting oxide was first modelled using Wagner's theory, assuming that both oxide surfaces are in equilibrium with the imposed gas atmospheres ($P_{O_2}^{rich} = P_{O_2}^{*rich}$ and $P_{O_2}^{lean} = P_{O_2}^{*lean}$) [Heyne, 1977; Wagner, 1957].

According to this theory, the steady oxygen permeation flux density j_{O_2} (in $mol.cm^{-2}.s^{-1}$) controlled by bulk diffusion in a mixed conductor is given by:

$$j_{O_2} = \frac{RT}{16F^2L}\int_{P_{O_2}^{lean}}^{P_{O_2}^{rich}} \frac{\sigma_i\sigma_e}{(\sigma_i+\sigma_e)}\, d\ln P_{O_2} \qquad (14)$$

where all the symbols have their original meaning and L is the membrane thickness.

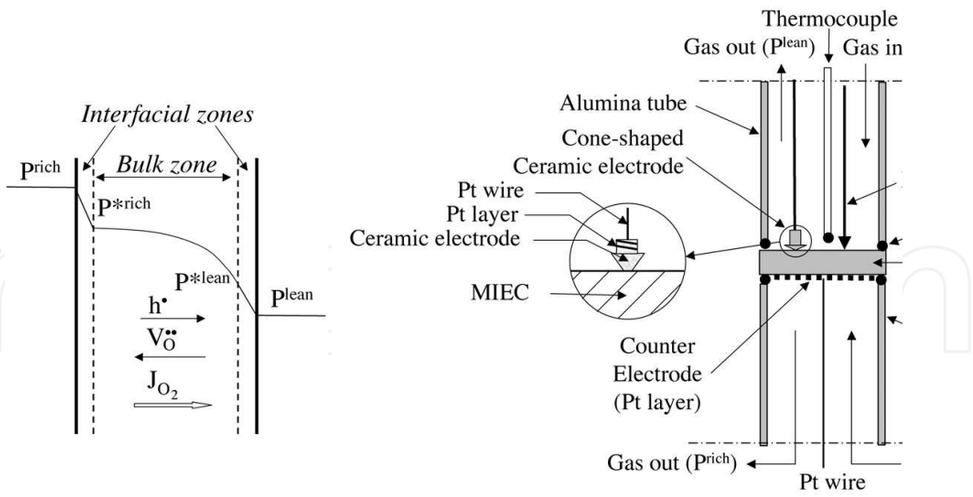

(a) (b)

Fig. 14. (a) Schematic drawing of the oxygen pressure gradients within a permeation membrane, (b) Permeation set-up, with magnified drawing of the ceramic point electrode.

In the case of mixed conductors in which the electronic conduction predominates, i.e., $\sigma_e >> \sigma_i$, the integral in the Wagner relation involves only σ_i over the oxygen partial pressure gradient:

$$j_{O_2} = \frac{RT}{16F^2L} \int_{P_{O_2}^{lean}}^{P_{O_2}^{rich}} \sigma_i \, d \ln P_{O_2} \tag{15}$$

Two cases can be considered:

- Taking an average value for σ_i or assuming σ_i to be constant simplifies the equation so that j_{O_2} is directly proportional to σ_i and $\ln\left(P_{O_2}^{rich} / P_{O_2}^{lean}\right)$:

$$j_{O_2} = \frac{RT\sigma_i}{16F^2L} \ln \frac{P_{O_2}^{rich}}{P_{O_2}^{lean}} = \frac{J_{O_2}}{L} \ln \frac{P_{O_2}^{rich}}{P_{O_2}^{lean}} \tag{16}$$

According to Möbius [Möbius, 1986], j_{O_2} is the oxygen permeation flux density and J_{O_2} is the specific oxygen permeability (in $mol.cm^{-1}.s^{-1}$).

- In case of simple defect model, neglecting the formation of defect association, the oxygen nonstoichiometry δ and the conductivity σ_i are proportional to $P_{O_2}^{1/n}$. Substitution into Eq. 15 with subsequent integration leads to a simplified expression for oxygen permeation:

$$J_{O_2} = \frac{\alpha}{L}\left[P_{rich}^{1/n} - P_{lean}^{1/n}\right] \text{ with } \alpha = \frac{RT\sigma_i^{\circ}}{16F^2} \tag{17}$$

σ_i° is the value of the ionic conductivity at unit oxygen pressure.

As indicated by Bouwmeester [Bouwmeester et al., 1994], for high values of n, Eq. (16) is obtained by expanding Eq. (17) as a power series and truncation after the first term.

Kleitz et al. [Kleitz et al., 1973; Fouletier et al., 1975] were the first to demonstrate that the existence of a nonvanishing semipermeability flux through a solid electrolyte induces a deviation from equilibrium on both sides of the membrane. They expanded the Wagner theory to account for partial control of surface reactions on the transport kinetics through stabilized zirconia. This approach has been applied to mixed ionic-electronic oxides [Bouwmeester et al., 1994; Chen et al., 1997; Geffroy et al., 2011; Xu & Thomson, 1999].

According to equation 16, in case of negligible effect of the surface exchange rate, the oxygen permeation flux density j_{O_2} is proportional to [ln(P^{rich}/P^{lean})], and the specific oxygen permeability J_{O_2} is independent of the membrane thickness [Kharton et al., 1999].

In case of limiting effect of the surface exchange rate, the specific oxygen permeability increases with the membrane thickness due to a decreasing role of the exchange kinetics (see Figure 15).

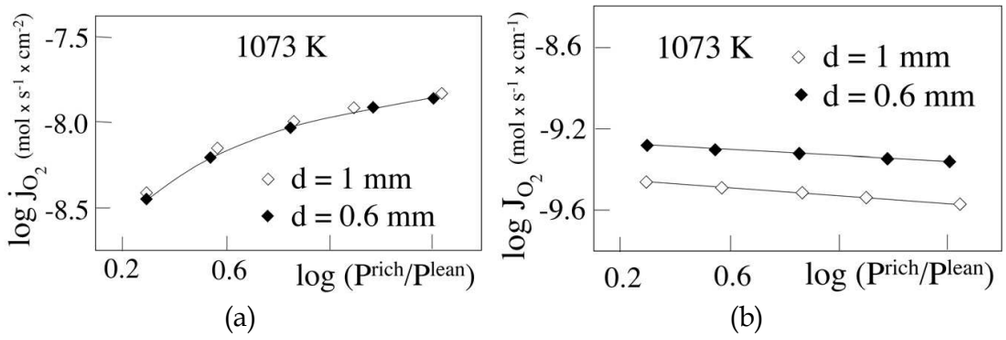

Fig. 15. (a): Variation of the oxygen permeation flux density (a) and of the specific oxygen permeability (b) with the oxygen pressure gradient, from [Kharton et al., 1999].

Another approach was to define the ratio h = k/D* where k is the surface exchange coefficient and D*, the tracer diffusion coefficient [Carter et al., 1992; Steele, 1992] or a critical thickness L_d (which is the reciprocal of the parameter h), at which the oxygen flux is half of that expected for a diffusion controlled process [Bouwmeester et al., 1994)]. The higher the L_d characteristic thickness (or the smaller the h value), the more the surface exchange contributes to the oxygen permeation flux. Examples of L_d values are given in [Gellings & Bouwmeester, 1997, p. 505]: L_d varies from 0.2 μm for $La_{0.5}Sr_{0.5}MnO_{3-\delta}$ to 0.03 cm for $La_{0.6}Sr_{0.4}Co_{0.4}Ni_{0.6}O_{3-\delta}$ at 700°C.

Oxygen permeation flux data for various MIECs have been recently compiled [Kharton, 1999; Sunarso et al., 2008].

The ionic conductivity can be deduced from the measured oxygen semipermeability flux using the following equation, in which the oxygen activities P* are taken into account instead of the oxygen pressures in the gas:

$$J_{O_2} = \frac{RT\sigma_i^{\circ}}{16F^2L}\left[P_{rich}^{*1/n} - P_{lean}^{*1/n}\right] \quad (18)$$

The oxygen activity on both sides of the pellet, i.e., $P_{O_2}^{*rich}$ and $P_{O_2}^{*lean}$, can be measured using ceramic point electrodes as described in section 2.2.1 [Geffroy et al., 2011; Mauvy et al., 2007].

Another approach has been to correlate the oxygen permeation flux to oxygen partial pressures [Xu & Thomson, 1999]. Assuming that the electronic conductivity is high and constant within the MIEC membrane, the oxygen flux can be written as;

$$J_{O_2} = \frac{D_V}{2L}\left([V_O^{\bullet\bullet}]^{lean} - [V_O^{\bullet\bullet}]^{rich}\right) \tag{19}$$

D_V is the diffusion coefficient of oxygen vacancies.

In case of mixed control of the oxygen flux (bulk diffusion and surface exchange), the concentration of oxygen vacancies at both faces of the membrane is governed by the reaction:

$$\frac{1}{2}O_2 + V_O^{\bullet\bullet} \xleftrightarrow{k_f, k_r} O_O^{\times} + 2h^{\bullet} \tag{20}$$

where k_f and k_r are the forward and reverse reaction rate constants.

Under stationary conditions, the oxygen permeation can be expressed as:

$$J_{O_2} = k_f\left(P^{rich}\right)^{1/2}\left[V_O^{\bullet\bullet}\right]^{rich} - k_r = k_r - k_f\left(P^{lean}\right)^{1/2}\left[V_O^{\bullet\bullet}\right]^{lean} \tag{21}$$

leading to:

$$J_{O_2} = \frac{D_V k_r\left[\left(P^{rich}\right)^{1/2} - \left(P^{lean}\right)^{1/2}\right]}{2Lk_f\left(P^{rich} \times P^{lean}\right)^{1/2} + D_V\left[\left(P^{rich}\right)^{1/2} + \left(P^{lean}\right)^{1/2}\right]} \tag{22}$$

The three parameters D_V, k_f and k_r can be estimated by fitting the experimental results as function the oxygen pressures on both sides of the membrane.

4.2 EMF – Faradic efficiency methods

The following cell has been used for the measurement of the ionic transport in a MIEC:

$$Pt, O_2 (P') / MIEC / Pt, O_2 (P'')$$

According to Wagner theory, the emf of the cell obeys the equation:

$$E = \frac{RT}{4F}\int_{P©}^{P''} t_{ion}\, d\ln P_{O_2} \tag{23}$$

where t_{ion} is the oxide ions transport number. In case of a pure ionic conductor, equation (23) becomes the Nernst law E_{th} (see equation (1)). Equation (23) can often be simplified as:

$$E = \bar{t}_{ion} E_{th} \quad (24)$$

where $\bar{t}_{ion}$ is the average ionic transference number.

This method has been applied to oxide electrolytes. However, it should be pointed out that the ionic transport number has to be not too small. In case of a non-stoichiometric oxide the resulting oxygen permeation flux will polarize one or both electrodes, and this method is not recommended.

The oxygen ionic transport number t_O can also be measured using the Faradic Efficiency method, i.e., t_O is the ratio between the oxygen ionic current and the total current driven through the sample by an applied electrical field. However, in case of noticeable electrode polarization, the measured transport number can differ from the actual value.

Kharton and co-workers [Kharton & Marques, 2001; Kharton et al., 2001; Kharton et al., 2007] have proposed modified EMF (EMF) and Faradic Efficiency (FE) methods and combination of these techniques (EMF-FE), taking into account the electrode polarization. The set-up is schematized in figure 16a. The cell includes an oxygen pump, an oxygen sensor and the studied membrane, all parts being separated by insulating layers. Figure 16b compares the results obtained with these techniques on $La_{0.9}Sr_{0.1}Ga_{0.8}Mg_{0.2}O_{3-\delta}$: due to polarization phenomena, the classical methods give an overestimated electronic transport number.

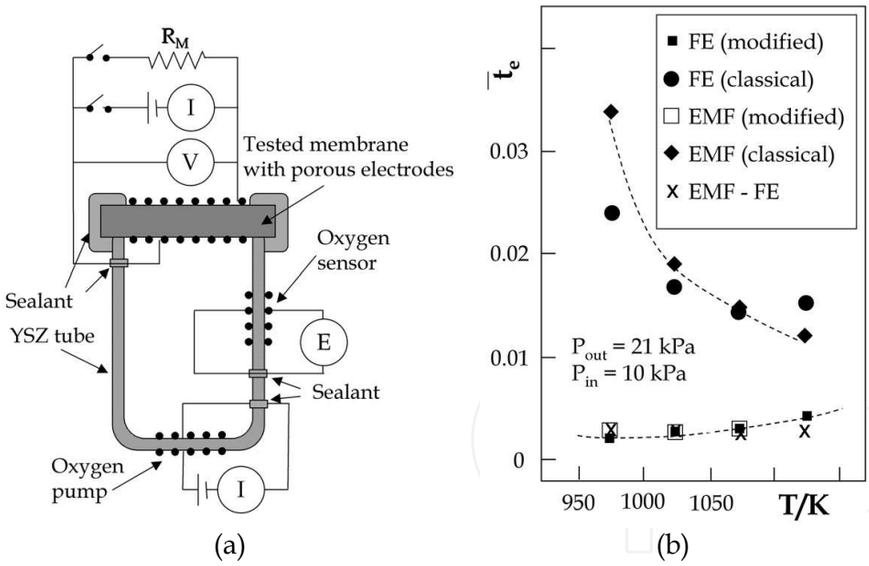

Fig. 16. (a): Electrochemical cells used for EMF and Faradic Efficiency measurements; (b) variation of the average electronic transport numbre of $La_{0.9}Sr_{0.1}Ga_{0.8}Mg_{0.2}O_{3-\delta}$ determined by different techniques, from [Kharton et al., 2007].

4.3 Patterson diagrams

This method was initially proposed by Patterson [Patterson, 1971]. It is based on the P_{O_2} dependence of the electrical conductivity. In Figure 17a is plotted the variation of log σ as functions of log (P_{O_2}) and of the reciprocal temperature. As shown in Figure 17b, at a given

temperature, three oxygen pressure domains can often be defined. In the medium oxygen pressure range, the conductivity is constant and $\sigma = \sigma_i$; at low P_{O_2}, the conductivity increase is ascribed to an additional n-type electronic conductivity ($\sigma = \sigma_i + \sigma_n$) and at high P_{O_2} the conductivity increase is due to an additional p-type conductivity ($\sigma = \sigma_i + \sigma_p$). Assuming that the ionic conductivity is constant over the whole oxygen pressure range, the partial electronic conductivity can be easily calculated.

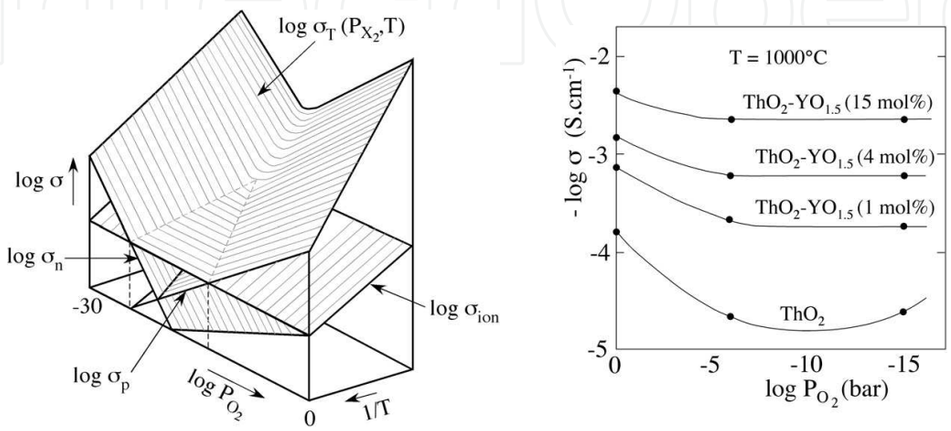

Fig. 17. (a): Schematic representation of log σ surfaces over log PO_2, 1/T space for $\sigma = \sigma_{ion}$, σ_n, σ_p and σ_{total}, from [Patterson, 1971]; (b): Log σ vs. log PO_2 for the system ThO_2-Y_2O_3.

This method can be considered as a fast and simple screening tool. It should be pointed out that the technique is convenient for electronic transport numbers higher than 1 % and when there is an oxygen partial pressure domain in which the conductivity is purely ionic.

4.4 Hebb-Wagner method

The Hebb-Wagner polarization technique has been developed either for the determination of electron and hole conductivity in ionic conductors [Hebb, 1952; Joshi & Wagner, 1975; Wagner, 1957] or for the measurement of ionic conductivity in MIECs [Riess, 1996; Wiemhöfer et al., 2002]. Basically, the method consists in using a reversible electrode and blocking electrodes to suppress the predominant charge carrier and thus enable measurement of the minority species. The main limitations of the method have been reviewed [Riess, 1996] and new experimental set-ups have been proposed.

The initially proposed cell is schematized in Figure 18a. Assuming that the MIEC is cationic conductor (mobile defects: $M_i^{\bullet}$), the interface M/MIEC (1) is a reversible electrode, and the interface C/MIEC (4) is an ion blocking electrode. The polarization of the voltage is chosen so that the mobile species tend to be depleted from the blocking electrode. Under steady-state condition, the ionic current is eliminated ($I = I_{el}$) and the theoretical I-V relation, according to the Wagner's theory is the following:

$$I = I_{el} = -\frac{RTS}{FL}\left[\sigma_e(0)\left(1 - e^{-\frac{FV}{RT}}\right) + \sigma_h(0)\left(e^{-\frac{FV}{RT}} - 1\right)\right] \quad (24)$$

$\sigma_e(0)$ and $\sigma_h(0)$ are the partial electron and hole conductivities in the MIEC at the interface (1), L and S are, respectively, the length and cross-sectional area of the MIEC.

By measuring the current through the MIEC sample and the applied voltage V, the electronic conductivity is determined.

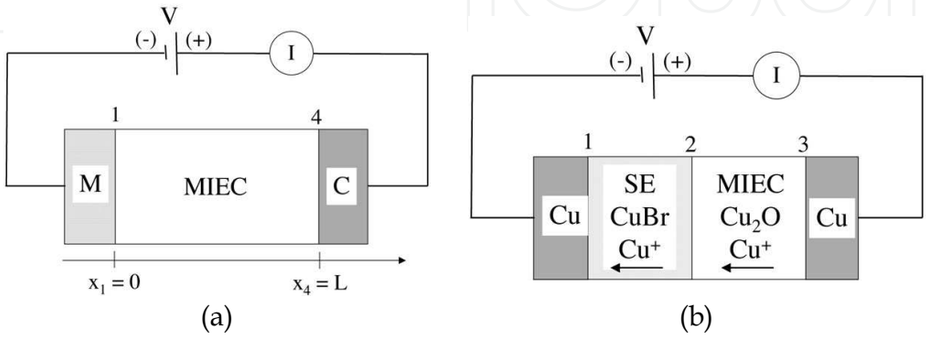

Fig. 18. (a): Two-point Hebb-Wagner polarization cell, C: ion-blocking electrodes, M: reversible electrode, MIEC: MIEC containing positive mobile ionic defects; (b): Two-point Hebb-Wagner polarization cell for the measurement of σ_i in Cu_2O from [Riess, 1992b].

An analogous method has been developed for determining the ionic conductivity in a MIEC. The blocking electrode for electronic defects is a solid electrolyte (SE), that conducts the same ions as the MIEC ($M_i^\bullet$ defects, is the experiment described, see Figure 18b):

(-) M/Solid Electrolyte ($M_i^\bullet$)/MIEC ($M_i^\bullet$, e', h$^\bullet$)/M (+)

Multi-electrode set-ups have been proposed by Riess, eliminating experimental problems such as errors due to overpotential at both electrodes or allowing the simultaneous measurement of σ_{el} and σ_i in a MIEC [Riess, 1992a, 1992b, 1996].

4.5 Short-circuit method ("zero driving force" method)

The ionic conductivity in a MIEC can be determined using the "short-circuiting" method [Riess, 1991]. Both electrodes are reversible systems with different compositions. The electronic current is brought to zero by short-circuiting the MIEC on a low impedance amperometer (V = 0). Consequently, it can be demonstrated that the ionic resistance R_i obeys the following equation [Riess, 1991]:

$$R_i = \frac{E_{th}}{I} \quad (25)$$

where E_{th} is the Nernst voltage determined by the compositions of the reversible electrodes, and I is the short-circuit current.

The main advantage of the method is that the contribution of electronic defects to the conductivity is eliminated without requirement of a blocking electrode. The sources of errors have been discussed [Riess, 1991, 1992b, 1997] and the method was applied to mixed conducting pyrochlores [Riess et al., 1992].

4.6 Conductivity vs. non-stoichiometry ratio

The electrical conductivity of electrochemically-reduced oxides is measured by impedance spectroscopy. The gas circuit is schematized in Figure 19a. During the first stage (indexes 1) the sample is reduced electrochemically (according to the procedure described in Section 3.2.3) and the stoichiometry ratio is determined using the oxygen sensor. Then the gas flowing in the experimental cell is purified using an oxygen getter (indexes 2). It has been checked that the sample composition remains constant over several days. The electrical conductivity of the reduced sample is measured as a function of temperature.

Figure 19b gives the Arrhenius plot of the electrical conductivity of stabilized zirconia (ZrO_2 - Y_2O_3, 12 m/o) as a function of the stoichiometry ratio.

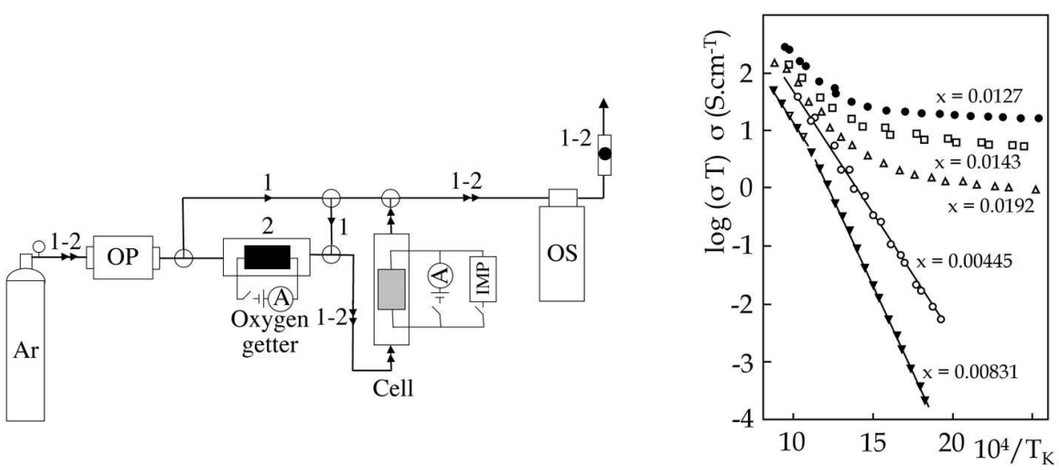

(a) (b)

Fig. 19. (a) Gas circuit, OP: oxygen pump, OS: oxygen sensor, IMP: impedancemeter, (1): reduction process, (2): conductivity measurement; (b) Arrhenius plot of the electrical conductivity for various non-stoichiometry ratio x (from Levy et al., 1988).

4.7 Relaxation methods

In chemical relaxation experiments, an abrupt change of chemical potential of one of the constituent elements, usually PO_2 for oxide materials is imposed on a sample under constant temperature. Physical properties such as weight and volume of the sample are recorded versus time until a new thermodynamically equilibrium state is reached. Because electrical conductivity is much more sensitive to change of oxygen chemical potential in the atmosphere than are the other properties as weight, considerable changes in conductivity can be observed even when the oxygen partial pressure change of the corresponding nonstoichiometry is very small. This makes the conductivity relaxation method more easily applicable to a wider variety of materials than other methods such as thermogravimetry

analysis [Lane et al., 2000; Ma et al. 1997; ten Elshof et al., 1997]. The transient behaviour in the re-equilibration process is recorded and analyzed by fitting the relaxation data to the solution of Fick's second law with appropriate boundary conditions [Crank, 1975].

A classical experimental setup, used for this type of study, is schematically drawn in Fig. 20a. Electrical conductivity relaxation experiments are performed using the four-probe method. Four platinum wires are connected to the sample using platinum paste (see Fig. 20b). Various atmospheres surrounding the sample are obtained by flowing a mixture of oxygen and nitrogen into the sample chamber, using two mass flow controllers or by introducing air. In both cases, the same flow rate is used. During the change of atmosphere, the flow rate is high enough to stabilize PO_2 inside the cell within a short duration compared with the relaxation time. Oxygen partial pressure steps of small amplitude are required to assign the relaxation process to a defined oxygen partial pressure. Moreover, this amplitude has to be small enough to assume constant the mobility of the defects during the relaxation process.

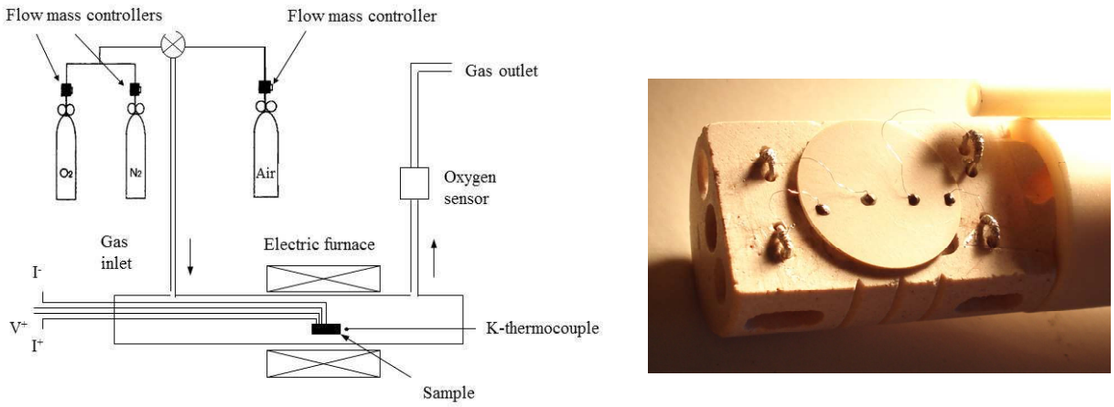

(a) (b)

Fig. 20. Schematic drawing of the experimental setup (a) and picture (b) of the 4-electrode sample holder.

In the case of $La_2Cu_{0.5}Ni_{0.5}O_{4+\delta}$ compound, oxygen is incorporated into the crystal lattice during the oxidation process or released from the lattice during the reduction step, as it can be observed on Fig. 21 when the sample is subjected to a sudden change of PO_2 [Mauvy et al., 2004].

During the relaxation process, nonstoichiometry spreads through the sample by lattice diffusion, which is driven by concentration gradients of defects. The ionic conductivity of $La_2Cu_{0.5}Ni_{0.5}O_{4+\delta}$ can only be contributed by oxygen vacancies ($V_O^{\bullet\bullet}$) and interstitial oxygen ions (O_i''). Theoretically, the oxygen vacancy concentration should decrease with increase in oxygen partial pressure. So, if the oxygen vacancy is the controlling defect, then one should expect the ionic conductivity to decrease with increase PO_2. However, experimental observations (see Fig. 21), indicate that ionic conductivity increases. This suggests that O_i'' is the predominant defect in this working conditions (high PO_2). Because the mobility of cationic defects is much lower than that of oxide defects and holes, chemical diffusion can be considered as the process of diffusion of interstitial oxide ions and counterdiffusion of holes.

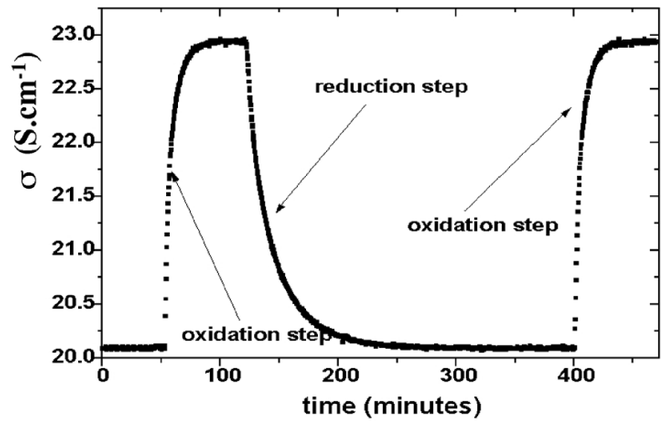

Fig. 21. Conductivity relaxation plots for $La_2Cu_{0.5}Ni_{0.5}O_{4+\delta}$ at 700°C for oxidation and reduction steps change in PO_2 between 0.21atm and 0.01atm.

The transient behaviour in the re-equilibration process can be described by the second Fick law [Sitte, 2001]. Taking into account the aspect ratio of the sample, the thickness of the pellet (slab like) controls the kinetic of the oxygen re-equilibration process. Consequently, the diffusion can be treated as a one-dimensional mechanism leading to the following equation:

$$\frac{dC}{dt} = \tilde{D}\frac{d^2C}{dx^2} \tag{26}$$

If the chemical diffusion is the rate-determining step, the following equation can be derived from the second Fick law, as suggested by Crank [Crank, 1975]:

$$\frac{M_t}{M_\infty} = 1 - \sum_{n=0}^{\infty} \frac{8}{(2n+1)^2\pi^2} \times \exp\left[-\frac{(2n+1)^2\pi^2\tilde{D}t}{4L^2}\right] \tag{27}$$

where L is the diffusion length and t the time. M_t / M_∞ represent the ratio of the mass of diffused oxide ions at time t, to that obtained for an infinite time.

Assuming constant the number of charges and the mobility of the charge carriers, the apparent conductivity is given by integrating the local conductivity all over the sample. Finally, the conductivity ratio can be directly related to the mass ratio:

$$\frac{M_t}{M_\infty} = \frac{\sigma_{app}(t) - \sigma_{app}(0)}{\sigma_{app}(\infty) - \sigma_{app}(0)} \tag{28}$$

In this formula σ(0), σ (t) and σ (∞) denote the apparent conductivity at t = 0 (initial), at time t (in the course of relaxation) and for t → ∞ (after reaching a new equilibrium state), respectively. The experimental data and the fitting curve in the form of fractional conductivity change as function of time are shown in Fig. 22. The chemical diffusion coefficient $\tilde{D}$ is then obtained by least-square fitting of the relaxation data.

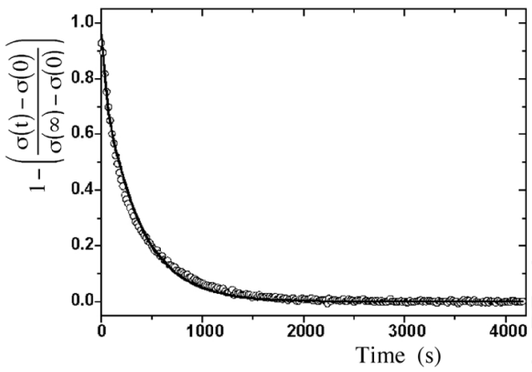

Fig. 22. Normalized and fitted conductivity data and fitting curve vs. time (at 700°C – PO_2 step from 0.01 atm to 0.21 atm).

Fig. 23 shows the Arrhenius plots of $\tilde{D}$ measured on two different samples of the same composition $La_2Cu_{0.5}Ni_{0.5}O_{4+\delta}$, but with two different thicknesses. Oxygen chemical diffusion coefficients, obtained for both samples, are equal over a wide temperature range. This observation confirms that the relaxation process is not controlled by the surface exchange, but by the bulk diffusion (i.e., this latter process is the limiting step).

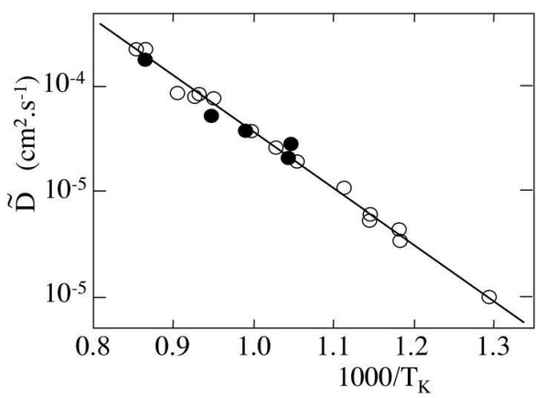

Fig. 23. Arrhenius plots of the oxygen chemical diffusion coefficient ($\tilde{D}$) measured on two samples with two different diffusion lengths: L_1 = 1.3mm (○) and L_2 = 0.7mm (●)

5. Conclusion

Determination of nonstoichiometry in oxides is a key point in the search for new materials for electrochemical applications. In recent decades, owing to their current and potential applications (electrodes in fuel cells, insertion electrodes, membranes of oxygen separation, gas sensors, catalytic materials, etc.), various methods of precise characterization of MIECs have been proposed, either the measurement of the defect concentrations and the stoichiometric ratio as functions of the oxide composition, of the surrounding oxygen pressure and of temperature, or the transport properties. There are different methods to determine the electrical properties of MIECs and, more specifically, the ionic and electronic contributions. The most appropriate method depends on different parameters, i.e., the total electrical conductivity of the studied oxides, the ionic and electronic transport numbers, the

temperature domain, etc. As examples, the characterization of solid electrolytes requires the determination of electronic transport numbers as low as 10^{-4}; oxygen leakage currents through interconnect materials in solid oxide fuel cells require the measurement of ionic conductivity in a practically pure electronic conductor; in ceramic membranes devoted to oxygen permeation, one of the most important criteria concerns the high ionic and electronic conductivities of the oxide. In the case of MIEC oxides used as oxygen electrode, the electro-catalytic activity is related to the properties of mixed conduction and, therefore, of non-stoichiometry. The determination of the level of ionic conductivity is fundamental for the material selection but this characterization is generally difficult to carry out because of the high electronic contribution to the total transport properties.

In this chapter all the proposed methods have not been described. The objective was to focus on the sources of errors, which may render the results useless. Deviation from equilibrium of the MIEC surface due to oxygen semipermeability flux can lead to erroneous measurements. Experimental set-ups, which allow overcoming these experimental difficulties, were described.

6. References

Akida, K.; Ueda, M.; Kawamura, K. & Maruyama, T. (2008). Continuous Monitoring of Oxygen Chemical Potential at the Surface of Growing Oxide Scales during High Temperature Oxidation of Metals, *Mater. Trans.* , Vol. 49, No 3, pp. 629-636

Bouwmeester, H.J.M.; Kruidhof, H.; Burggraaf, A.J. & Gellings, P.J. (1992). Oxygen semipermeability of erbia-stabilized bismuth oxide, *Solid State Ionics*, Vol. 53-56, pp. 460-468

Bouwmeester, H.J.M.; Kruidhof, H. & Burggraaf, A.J. (1994). Importance of the surface exchange kinetics as rate limiting step in oxygen permeation through mixed-conducting oxides, *Solid State Ionics*, Vol. 72, pp. 185-194

Caneiro, A.; Bonnat, M. & Fouletier, J. (1981). Measurement and regulation of oxygen content in gases using solid electrolyte cell, IV - Accurate preparation of CO_2-CO and H_2O-H_2 mixtures, *J. Applied Electrochem.*, Vol. 11, pp. 83-90

Caneiro, A.; Bavdaz, P.; Fouletier, J. & Abriata, J.P. (1982). Adaptation of an electrochemical system for measurement and regulation of oxygen partial pressure to a symmetrical thermogravimetric analysis system developed using a Cahn 1000 electrobalance, *Rev. Sci. Instrum.*, Vol. 53, pp. 1072-1075

Caneiro, A.; Mogni, L.; Grunbaum, N. & Prado, F. (2011). Physicochemical properties of non-stoichiometric oxides - Mixed conductors, Part I & II, *J. Therm. Anal. Calorim.*, Vol. 103, pp. 597-606 & Vol. 104, pp. 781-788

Carter, S.; Selcuk, A.; Chater, R.J.; Kajida, J.; Kilner, J.A. & Steele, B.C.H. (1992). Oxygen transport in selected nonstoichiometric perovskite-structure oxides, *Solid State Ionics*, Vol. 53-56, pp. 597-605

Chen, C.H.; Bouwmeester, H.J.M., van Doorn, R.H.E., Kruidhof, H. & Burggraaf, A.J. (1997). Oxygen permeation of $La_{0.3}Sr_{0.7}CoO_{3-d}$, *Solid State Ionics*, Vol. 98, pp. 7-13

Crank, C. (1975). *The mathematics of diffusion*, 2nd Edn., Clarendon Press, Oxford, pp.44-68

Ducroux, R.; Fromont, M.; Jean Baptiste, Ph. & Pattoret, A. (1980). Mesures en continu de la redistribution de l'oxygène sous gradient thermique dans UO_{2+x}, *J. Nucl. Mat.*, Vol. 92, pp. 325-333

Ducroux, R. & Jean Baptiste, Ph. (1981). Mesure du potentiel d'oxygène dans le système $U_{0.7}Ce_{0.3}O_{2+x}$ à l'aide d'une minisonde à électrolyte solide, *J. Nucl. Mat.*, Vol. 97, pp. 333-336

Fouletier, J.; Fabry, P. & Kleitz, M. (1976). Electrochemical semipermeability and the electrode microsystem in solid oxide electrolyte cells, *J. Electrochem. Soc.*, Vol. 123, pp. 204-213

Fouletier, J. & Kleitz, M. (1978). Direct determination of the electrical conductivity-non stoichiometry relationship in ionically-conducting metallic oxides, *J. Electrochem. Soc.*, Vol. 125, pp. 751-755

Fouletier, J. & Vitter, G. (1980). Gaseous oxygen gauges : characteristics and applications, In: *Applications of Solid Electrolytes*, T. Takahashi, A. Kozawa (Eds.), pp. 108-113, JEC Press Inc., Cleveland

Fouletier, J.; Vitter, G. & Kleitz, M. (1981). Measurement and regulation of oxygen content in gases using solid electrolyte cells, III - Oxygen pump-gauge, *J. Applied Electrochem.*, Vol. 5, pp. 111-120

Fouletier, J.; Meas, Y.; Fouletier, M. & Kleitz, M. (1982). Oxidation studies at constant oxygen pressure or constant oxidation rate, In: *Reactivity of Solids*, Vol. 1, K. Dyrek, J. Haber, J. Nowotny (Eds.) , p. 138-144, Elsevier, ISBN 83-01-03585-4, Amsterdam

Fouletier, J. (1982/83). Gas analysis with potentiometric gas sensors, *Sensors and Actuators*, Vol. 3, pp. 295- 314

Fouletier, J.; Siebert, E. & Caneiro, A. (1984). Accurate monitoring of low oxygen activity in gases with conventional oxygen gauges and pumps, In: *Science and Technology of Zirconia II*, Adv. In Ceram., Vol. 12, N. Claussen et al. (Eds.), pp. 618-626, Am. Ceram. Soc., Columbus

Geffroy, P.M.; Vivet, A.; Fouletier, J.; Richet, N.; Del Gallo, P. & Chartier, T. (2011). Influence of Oxygen Surface Exchange on Oxygen Semi-Permeation through $La_{1-x}Sr_xFe_{1-y}Ga_yO_{3-\delta}$ Dense Membrane, *J. Electrochem. Soc.*, Vol. 158, No 8, pp. B971-B979

Gellings, P.J. & Bouwmeester, H.J.M. (Eds). (1997). *The CRC Handbook of Solid State Chemistry*, CRC Press, ISBN 0-8493-8956-9, London

Hebb, M.C. (1952). Electrical Conductivity of Silver Sulfide, *J. Chem. Phys.*, Vol. 20, pp. 185-190

Heyne, L. (1977). Electrochemistry of Mixed Ionic-Electronic Conductors, In: *Solid Electrolytes*, Topics in Applied Physics, S. Geller (Ed.), p. 169-221, Springer, Berlin

Joshi, A.V.; Wagner Jr., J.B. (1975). Electrochemical Studies on Single Crystalline CuCI Solid Electrolyte, *J. Electrochem. Soc.*, Vol. 122, pp. 1071-1080

Kharton, V.V.; Yaremchenko, A.A.; Kovalevsky, A.V.; Viskup, A.P.; Naumovich, E.N. & Kerko, P.F. (1999). Perovskite-type oxides for high-temperature oxygen separation membrane, *J. Memb. Sci.*, Vol. 163, pp. 307-317

Kharton, V.V. &, Marques, F.M.B. (2001). Interfacial effects in electrochemical cells for oxygen ionic conduction measurements - I. The e.m.f. method, *Solid State Ionics*, Vol. 140, pp. 381-394

Kharton, V.V.; Viskup, A.P.; Figueiredo, F.M.; Naumovich, E.N. Yaremchenko, A.A. & Marques, F.M.B. (2001). Electron-hole conduction in Pr-doped $Ce(Gd)O_{2-\delta}$ by faradaic efficiency and emf measurements, *Electrochim. Acta.*, Vol. 46, pp. 2879-2889

Kharton, V.V.; Shaula, A.L. & Marques, M.F.B. (2007). Oxygen ion transport number: assessment of combined measurement methods, *Ionics*, Vol. 13, pp. 163-171

Kharton, V.V. ; Tsipis, E.V. ; Naumovich, E.N. ; Thursfield, A. ; Patrakeev, M.V. ; Kolotygin, V.A. ; Waerenborgh, J.C. & Metcalfe, I.S. (2008). Mixed conductivity, oxygen permeability and redox behavior of K_2NiF_4-type $La_2Ni_{0.9}Fe_{0.1}O_{4+\delta}$, *J. Solid State Chem.*, Vol. 181, pp. 1425-1433

Kiukkola, K.; Wagner, C. (1957). Measurements on galvanic Cells Involving Solid Electrolytes, *J. Electrocheml. Soc.*, Vol. 104, No 6, pp. 379-387

Kleitz, M.; Siebert, E.; Fabry, P. & Fouletier, J. (1992). Solid State Electrochemical Sensors, In: *Sensors - A Comprehensive Survey*, W. Göpel, J. Hesse, J.N. Zemel (Eds), Chemical and Biochemical Sensors, Part I, Vol. 2, pp. 341-428, VCH, ISBN 3-527-26768-9, Weinheim

Lane, J.A. & Kilner, J.A. (2000). Measuring oxygen diffusion and oxygen surface exchange by conductivity, *Solid State Ionics*, Vol. 136-137, pp. 997-1001

Lankhorst, M.H.R. & Bouwmeester, H.J.M. (1997). Determination of Oxygen Nonstoichiometry and Diffusivity in Mixed Conducting Oxides by Oxygen Coulometric Titration, *J. Electrochem. Soc.*, Vol. 144, No 4, pp. 1261-1267

Levy, M.; Fouletier, J. & Kleitz, M. (1988). Model for the electrical conductivity of reduced stabilized zirconia, *J. Electrochem. Soc.*, Vol. 135, pp. 1584-1589

Mari, C.M.; Pizzini, S.; Manes, L. & Toci, F. (1977). A Novel Approach to the Oxygen Activity Microdetermination of Oxides by EMF Measurements, *J. Electrochem. Soc.*, Vol. 124, No 12, pp. 1831-1836

Mauvy, F.; Bassat, J.M.; Boehm, E.; Dordor, P.; Grenier, J.C. & Loup, J.P. (2004). Chemical oxygen diffusion coefficient measurement by conductivity relaxation - Correlation between tracer diffusion coefficient and chemical diffusion coefficient, *J. Eur. Ceram. Soc.*, Vol. 24, pp. 1265-1269

Mauvy, F.; Boehm, E.; Bassat, J.M.; Grenier, J.C. & Fouletier, J. (2007). Oxygen permeation fluxes through $La_2Cu_{0.5}Ni_{0.5}O_{4+\delta}$ dense ceramics: comparison with oxygen diffusion coefficients, *Solid State Ionics*, Vol. 178, pp. 1200-1204

Mauvy, F.; Lalanne, C.; Bassat, J.M.; Grenier, J.C.; Brisse, A., Sauvet, A.L.; Barthet, C. & Fouletier, J. (2009). Electrochemical study of the $Nd_{1.95}NiO_{4+\delta}$ oxide electrolyte interface, *Solid State Ionics*, Vol. 180, pp. 1183-1189

Meas, Y.; Fouletier, J.; Passelaigue, D. & Kleitz, M. (1978). Nouveau montage d'étude des réactions d'oxydation à pression d'oxygène constante, *J. Chim. Phys.*, Vol. 75, pp. 826-834

Mizusaki, J, Tagawa, H, Naraya, K & Sasamoto, T. (1991). Nonstoichiometry and thermochemical stability of the perovskite-type $La_{1-x}Sr_xMnO_{3-\delta}$, *Solid State Ionics*, Vol. 49, pp. 111-118

Möbius, H.H. (1986). Oxygen Current Density Coefficient of Oxidic Materials as a Parameter for Selection and Development of Electrodes with Solid Electrolytes, Extended Abstracts of the *37th Meeting ISE, Int. Soc. of Electrochem.*, Vilnius, USSR, Vol. 1, p. 136-139

Nakamura, A. & Fujino, T. (1987). Thermodynamic study of UO_{2+x} by solid state emf technique, *J. Nucl. Mat.*, Vol. 149, No 1, pp. 80-100

Nakamura, T., Yashiro, K., Sato, K & Mizusaki, J. (2009a). Oxygen nonstoichiometry and chemical stability of $Nd_{2-x}Sr_xO_{4+\delta}$, *J. Solid State Chem.*, Vol. 182, pp. 1533-1537

Nakamura, T., Yashiro, K., Sato, K & Mizusaki, J. (2009b). Oxygen nonstoichiometry and defect equilibrium in $La_{2-x}Sr_xO_{4+\delta}$, *Solid State Ionics*, Vol. 180, pp. 368-376

Otobe, H.; Akabori, M. & Arai, Y. (2009). Oxygen potential measurements of $Am_{0.5}Pu_{0.5}O_{2-x}$ by EMF method, *J. Nucl. Mat.*, Vol. 389, pp. 68-71

Panlener, R.J.; Blumenthal, R.N., Garnier, J.E. (1975). A Thermodynamic Study of Nonstoichiometric Cerium Oxide, *J. Phys. Chem. Solids*, Vol. 36, No 11, pp. 1213-1222

Porat, O.; Riess, I. (1994) Defect chemistry of $Cu_{2-y}O$ at elevated temperatures. Part. I: Non-stoichiometry, phase width and dominant point defects, *Solid State Ionics*, Vol. 74, pp. 229-238

Rickert, H. (1982). *Electrochemistry of Solids - An introduction*, Springer-Verlag, ISBN 0-387-11116-6, Berlin

Riess, I. & D.S. Tannhauser, D.S. (1982). Control and measurement of stoichiometry in oxides, In: *Reactivity of Solids*, Vol. 1, K. Dyrek, J. Haber, J. Nowotny (Eds.), Elsevier, pp. 503-517

Riess, I. (1991). Measurement of electronic and ionic partial conductivities in mixed conductors without the use of blocking electrodes, *Solid State Ionics*, Vol. 44, pp. 207-214

Riess, I. (1992). Four point Hebb-Wagner polarization method for determining the electronic conductivity in mixed ionic-electronic conductors, *Solid State Ionics*, Vol. 51, No 3-4, pp. 219-229

Riess, I. (1992b). Recent investigations into the properties of mixed ionic electronic conductors, In: *Solid State Ionics*, Balkanski, M.; Takahashi, T. & Tuller, H.L. (Eds.), pp. 475-485, Elsevier, ISBN 0-444-89354-7, Amsterdam

Riess, I.; Kramer, S. & Tuller, H.L. (1992). Measurement of ionic conductivity in mixed conducting pyrochlores by short circuit method, In: *Solid State Ionics*, Balkanski, M.; Takahashi, T. & Tuller, H.L. (Eds.), pp. 499-505, Elsevier, ISBN 0-444-89354-7, Amsterdam

Riess, I.; Safadi, R. & Tuller, H.L. (1994). Problems with Hebb-Wagner polarization measurements due to overpotentials and decomposition of the sample, *Solid State Ionics*, Vol. 72, pp. 3-6

Riess, I. (1996). Review of the limitation of the Hebb-Wagner polarization method for measuring partial conductivities in mixed ionic electronic conductors, *Solid State Ionics*, Vol. 91, pp. 221-232

Riess, I. (1997). Electrochemistry of mixed ionic-electronic conductors, In: *The CRC Handbook of Solid State Chemistry*, Gellings, P.J. & Bouwmeester, H.J.M. (Eds), pp. 223-268, CRC Press, ISBN 0-8493-8956-9, London

Shores, D.A.; Rapp, R.A. (1971). Solid Bielectrolyte Cells for Thermodynamic Measurements, *J. Electrochemical Soc.*, Vol. 118, No 7, pp.1107-1111

Sitte, W., Bucher, E.,Benisik A; Preis W., (2001) Oxygen nonstoichiometry and ionic transport properties of $La_{0.4}Sr_{0.6}CoO_{3-\delta}$. *Spectrochimica Acta*, 2001, Part A57, 2071-2076

Sorensen T.O. (Ed.). (1981). *Nonstoichiometric oxides*, Academic Press, ISBN 0-12-655280-0, London

Sunarso, J.; Baumann, S.; Serra, J.M.; Meulenberg, W.A.; Liu, S.; Lin, Y.S. & Diniz da Costa, J.C. (2008). Mixed ionic-electronic conducting (MIEC) ceramic-based membranes for oxygen separation, *J. Memb. Sci.*, Vol. 320, pp. 13-41

ten Elshof, J.E.; Lankkhorst, M.H.R. & Bouwmeester, H.J.M. (1997). Chemical diffusion and oxygen exchange of $La_{0.6}Sr_{0.4}Co_{0.6}Fe_{0.4}O_{3-\delta}$, *Solid State Ionics*, Vol. 99, pp. 15-22

Tretyakov, J.D. & Muan, A. (1969). A New Cell for Electrochemical Studies at Elevated Temperatures Design and Properties of a Cell Involving a Combination of Thorium Oxide-Yttrium Oxide and Zirconium Oxide-Calcium Oxide Electrolytes, *J. Electrochem. Soc.*, Vol. 116, No 3, pp. 331-334

Tretyakov, J.D., Maiorova, A.F. & Berezovskaya, Y.M. (1997). Electrochemical Titration in Study of Nonstoichiometric Compounds, *Key Engineering Materials*, Vol. 125-126, pp. 283-316

Tsipis, E.V.; Naumovich, E.N. ; Shaula, A.L. ; Patrakev, M.V. ; Waerenborgh, J.C. & Kharton, V.V. (2008). Oxygen nonstoichiometry and ionic transport in $La_2Ni_{0.9}Fe_{0.1}O_{4+\delta}$, *Solid State Ionics*, Vol. 179, pp. 57-60

Patrakeev, M.V.; Leonidov, I.A. ; Lakhtin, A.A. & Kozhevnikov, V.L. (1995), Oxygen Nonstoichiometry of $(Nd_{2/3}Ce_{1/3})_4(Ba_{2/3}Nd_{1/3})_4Cu_6O_{16+x}$, *J. Solid State Chem.*, Vol. 120, pp. 146-150

Une, K. & Oguma, M. (1982). Thermodynamic properties of nonstoichiometric urania-gadolinia solid solutions in the temperature range 700-1100°C, *J. Nucl. Mat.*, Vol. 110, pp. 215-222.

Wagner, C. (1957). Galvanic Cells with Solid Electrolytes Involving Ionic and Electronic Conduction, In: *Proceedings of the International Committee Electrochemical Thermodynamics and Kinetics*, Chap. 8.5, 7th C.I.T.C.E. Meeting, 1955, Butterworths, London, pp. 361-377

Wagner, C. (1971). The determination of small deviations from the ideal stoichiometric composition of ionic crystals and other binary compounds, *Progress in Solid State Chemistry*, vol.6, pp. 1-15

Weppner, W.; Huggins, R.A. (1978). Electrochemical methods for determining kinetic properties of solids, *Ann. Rev. Mater. Sci.*, Vol. 8, pp. 269-311

Wiemhöfer, H.D.; Bremes, H.G.; Nigge, U. & Zipprich, W. (2002). Studies of ionic transport and oxygen exchange on oxide materials for electrochemical gas sensors, *Solid State Ionics*, Vol. 150, pp. 63-77

Xu, S.J. & Thomson, W.J. (1999). Oxygen permeation rates through ion-conducting perovskite membranes, *Chem. Eng. Sci.*, Vol. 54, pp. 3839-3850

Zhao, H.; Mauvy, F.; Bassat, J.M.; Fourcade, S.; Lalanne, C.; Boehm, E. & Grenier, J.C. (2008). New cathode materials for IT-SOFC: phase stability, oxygen exchange and cathode properties of $La_{2-x}NiO_{4+\delta}$, *Solid State Ionics*, Vol. 179, pp. 2000-2005

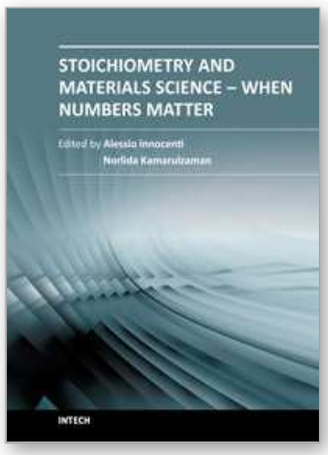

Stoichiometry and Materials Science - When Numbers Matter

Edited by Dr. Alessio Innocenti

ISBN 978-953-51-0512-1
Hard cover, 436 pages
Publisher InTech
Published online 11, April, 2012
Published in print edition April, 2012

The aim of this book is to provide an overview on the importance of stoichiometry in the materials science field. It presents a collection of selected research articles and reviews providing up-to-date information related to stoichiometry at various levels. Being materials science an interdisciplinary area, the book has been divided in multiple sections, each for a specific field of applications. The first two sections introduce the role of stoichiometry in nanotechnology and defect chemistry, providing examples of state-of-the-art technologies. Section three and four are focused on intermetallic compounds and metal oxides. Section five describes the importance of stoichiometry in electrochemical applications. In section six new strategies for solid phase synthesis are reported, while a cross sectional approach to the influence of stoichiometry in energy production is the topic of the last section. Though specifically addressed to readers with a background in physical science, I believe this book will be of interest to researchers working in materials science, engineering and technology.

INTECH
open science | open minds

InTech Europe
University Campus STeP Ri
Slavka Krautzeka 83/A
51000 Rijeka, Croatia
Phone: +385 (51) 770 447
Fax: +385 (51) 686 166
www.intechopen.com

InTech China
Unit 405, Office Block, Hotel Equatorial Shanghai
No.65, Yan An Road (West), Shanghai, 200040, China
中国上海市延安西路65号上海国际贵都大饭店办公楼405单元
Phone: +86-21-62489820
Fax: +86-21-62489821

IntechOpen